

Experimental assessment of the seismic response of three-leaf stone masonry walls, with due consideration to soil–structure interaction

A.-A. Manoledaki, V. Drosos, I. Anastasopoulos, E. Vintzileou & G. Gazetas

National Technical University of Athens, Greece



SUMMARY:

The out-of-plane seismic response of historic stone masonry walls is investigated herein, with due consideration to soil–foundation–structure interaction (SFSI). A series of pushover tests were performed on reduced scale (1:3) wall specimens, which consisted of a three-leaf stone masonry built on top of a spread footing. The walls were subjected to out-of-plane displacement, imposed at mid-height. Initially, a set of experiments were conducted ignoring SFSI. Then, the specimens were founded on a sand layer to examine the role of SFSI. Two idealized soil deposits were modelled: (a) dense sand of relative density $D_r = 92\%$, and (b) loose sand of relative density $D_r = 33\%$. The results are discussed in terms of force–displacement response, failure modes (crack patterns, soil deformation), and footing settlement–rotation response. It is shown that the performance of the walls is substantially affected by SFSI effects, as well as by the boundary conditions.

Keywords: Out-of-plane, Pushover testing, Soil–structure interaction, Stone masonry walls, rocking

1. INTRODUCTION

Three-leaf stone masonry is a structural typology commonly encountered in monumental structures and urban nuclei historic buildings. Typically, such constructions are one or two storeys high and employ timber floors and roof. The structural system consists of 40 cm to 60 cm thick stone masonry walls, uniformly distributed in both directions. The foundation is typically shallow, and comprises of spread footings that run along the entire length of the walls. Their overall seismic response is quite complex, especially when considering soil–foundation–structure interaction (SFSI). Therefore, it seemed reasonable to begin by examining the response of single structural components, namely stone masonry walls. Acknowledging that such walls exhibit enhanced vulnerability against seismic actions perpendicular to their plane, the experimental research presented herein focuses on their *out-of-plane* seismic response, with due consideration to SFSI effects.

A review of the published literature on out-of-plane tests reveals a restricted number of studies concerning contemporary brick masonry walls (Derakhshan and Ingham, [2008]; Griffith et al., [2004] and [2007]; Kanit and Atimtay, [2006]; Meisl et al., [2007]; Wilhelm et al., [2007]), and/or contemporary block masonry walls (ABK, [1981]). However, to the best of our knowledge, no out-of-plane tests on historic stone masonry walls had been performed prior to this research. This is also the first time that soil–structure interaction issues are being addressed. An overview of the obtained experimental results is presented and discussed, in terms of force–displacement response, footing settlement–rotation response, and observed failure modes (wall crack patterns and soil deformation).

2. SPECIMEN DESCRIPTION

The specimens represent walls typically found in historic three-leaf stone masonry structures. A reduced scale of 1:3 was adopted for the tests. As can be seen in Figure 1, each wall specimen (0.5 m

long, 0.2 m thick and 1.0 m high) was built on top of a spread concrete footing (0.5 m long, 0.3 m wide and 0.1 m high) which ran along the entire wall length.

The walls were constructed by a professional mason, following the traditional building procedure. They consist of two external leaves, built simultaneously as separate walls, and a loose poor quality incoherent inner core. The external leaves were made of nine courses of rubble limestone bonded with lime-pozzolan based mortar. As confirmed by the results of the conducted standardized tests, the constitutive materials were representative of those found in historic structures. The infill material was prepared on site by mixing stone fragments with binding mortar. Subsequently, it was poured in the gap between the external leaves without compaction, thereby achieving a voids ratio of 40% to 45%. The leaves had approximately the same thickness (i.e., $t_w/3 = 6.67$ cm), and no transversal connection was provided between them (non-monolithic behavior within the wall thickness).

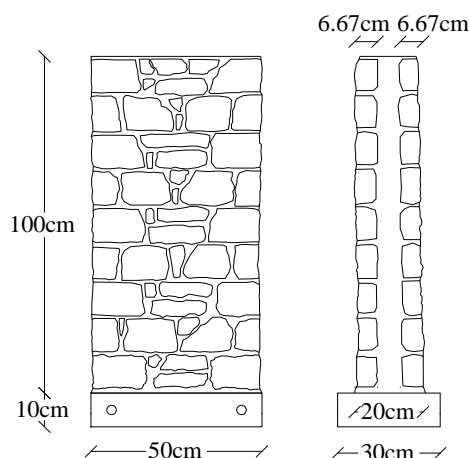


Figure 1. Schematic geometry of the test specimens.

3. EXPERIMENTAL PROGRAM

All tests were conducted at the facilities of the NTUA Soil Mechanics Laboratory. As presented in Table 1, the experimental program was divided in two phases. The initial phase involved a set of pushover tests ignoring SFSI. Then, during the second phase, the specimens were founded on a dry sand layer pluviated inside a rigid soil container, so as to investigate the role of SFSI. *Longstone* sand, an industrially produced fine and uniform quartz sand with $D_{50} = 0.15$ mm and uniformity coefficient $C_u = 1.42$ was used in the experiments. Its characteristics have been documented in Anastasopoulos et al., [2010]. The sand was pluviated through an electronically-controlled sand raining system, capable of producing sand specimens of controllable relative density D_r . Two idealized soil deposits were modelled, in order to examine the effect of soil resilience: (a) dense sand of $D_r = 92\%$, and (b) loose sand of $D_r = 33\%$. Monotonic and cyclic out-of-plane loading was imposed at wall mid-height, by means of a servo-electric screw-jack actuator. Tests were performed under displacement control, at an increment rate of 0.2 mm/s. The prescribed cyclic displacement protocols are given in Figure 2.

Table 1. Experimental program.

Phase	Specimen	Test type	SFSI	D_r (%)	Strengthening
I	W1	Monotonic	No	–	No
	W2	Cyclic	No	–	No
	W3	Monotonic	No	–	Yes
II	W4	Cyclic	Yes	92	No
	W5	Cyclic	Yes	33	No

While most of the specimens were tested as built, specimen W3 was tested in strengthened condition. Strengthening against out-of-plane bending was imposed through a post-tensioning system (see Figure 3) which induced a couple of constantly monitored resisting forces.

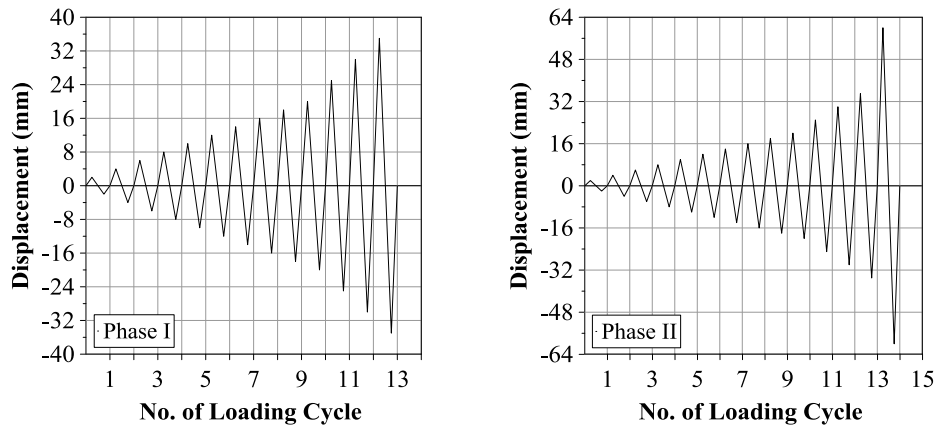


Figure 2. Cyclic loading displacement histories.

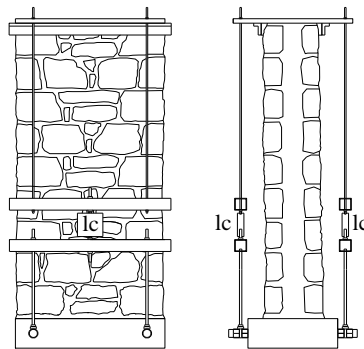


Figure 3. Post-tensioning system used to strengthen specimen W3.

4. TEST SET-UP

Depending on the features of the stone masonry structure, in reality, there is a certain degree of variability regarding the translational and rotational restraint provided to the walls. It is well known that timber floors and roof do not represent a *rigid* diaphragm, and do not provide fixed connection with the walls. Hence, for accurate more realistic representation of the wall boundary conditions typically encountered in historic structures an adjustable test rig was expressly designed to allow rotation of the wall crest while restrain its translational motion. The sensitivity of the out-of-plane response against wall boundary conditions was examined through the subsequently presented two cases. The test rig configuration used during phase I (see Figure 4a) aimed at representing the case of walls whose elongation is partially obstructed by the floor or roof. In phase II, as can be seen in Figure 4b, two essential alterations were made at the test rig: (a) the wall–footing specimen was founded directly on the sand layer, and (b) the top support was modified to allow for vertical movement due to footing settlement. It should be noted that all the walls were free along their vertical edges.

Regarding the instrumentation, wall displacements were recorded by nine wire displacement transducers (wdt's) mounted on a stationary frame (see Figure 4c). In particular, horizontal displacements were measured at key locations along the wall height (i.e., at courses 1, 3, 5, 7 and 9), while vertical displacements were measured at two points at both the footing and the wall crest so that the rotation of the wall ends to be estimated. The force applied by the actuator was measured using a load cell (lc). In the case of the strengthened specimen W3, two additional load cells were attached to

the post-tensioning system in order to monitor the couple of developing forces. Soil–foundation interaction was monitored at all times, through the transparent soil container, via a digital camera. The post-test surface relief of the sand layer was obtained with the help of a laser displacement transducer (ldt) travelling above the surface along the mid-axis of the footing.

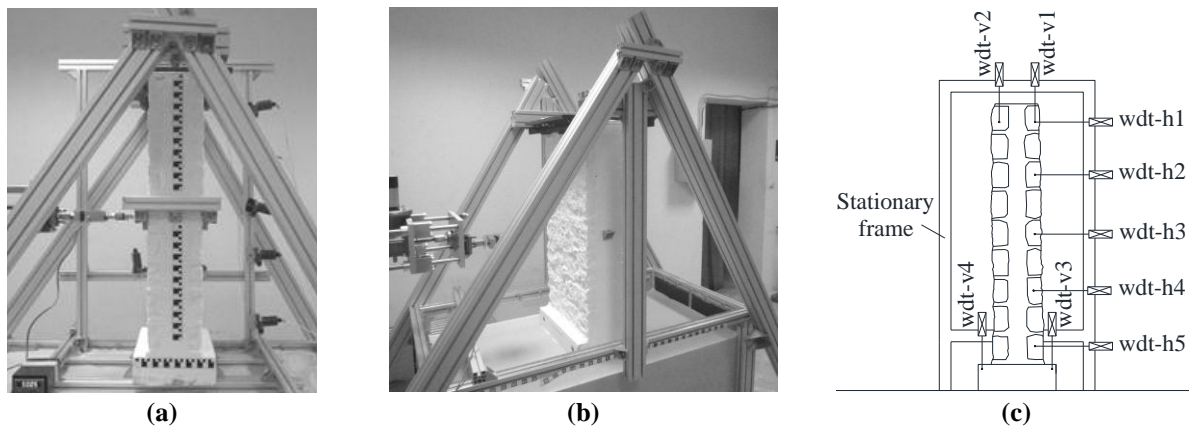


Figure 4. Test set-up: (a) phase I configuration, (b) phase II configuration, and (c) wdt's arrangement.

5. TEST RESULTS

5.1. Phase I tests: ignoring SFSI

The results of phase I tests are summarized in Figure 5. The resisting force is plotted against the applied displacement at wall mid-height. For comparison purposes, common axis scales were used for specimens W1 (monotonic test) and W2 (cyclic test), which were tested as built. The data are also summarized in Table 2.

Inspection of the force–displacement curves indicates a consistency in the general response trends of control specimens W1 and W2. The onset of cracking (F_{cr} , Δ_{cr}), at the extreme tensile fibers of the critical section, signified the end of the initial linear-elastic response stage. Afterwards, the walls continued to resist with increasing force and degrading stiffness, until peak force (F_{max} , $\Delta_{F_{max}}$) was reached. This increased flexural bending resistance is attributed to the beneficial effect of the axial load induced by the top support which restrains the vertical movement. In the course of the test, while imposed displacement amplitude progressively increased, the wall had the tendency to elongate (due to arching). However, as it was partially restrained by the top support, it was subjected to an additional axial load which resulted in higher axial strength. The significant effect of boundary conditions on the out-of-plane response of the tested walls becomes even more evident when the attained F_{cr} and F_{max} values are compared.

In the case of the cyclically loaded specimen W2, there is an obvious asymmetry of the force–displacement data in the positive and negative displacement directions. This could be attributed to the fact that cracking initiated earlier in the positive displacement direction (i.e., an entire loading cycle ahead) and therefore, as a result of the higher damage accumulation level, the respective wall side was weakened more rapidly.

The force–displacement response of the strengthened specimen W3 was substantially improved, due to the couple of resisting forces induced by the post-tensioning system. As shown by the test results (Figure 5; Table 2), its out-of-plane resistance was practically doubled in comparison with control specimens W1 and W2. Hence, the specific strengthening technique proved to be highly effective against out-of-plane actions.

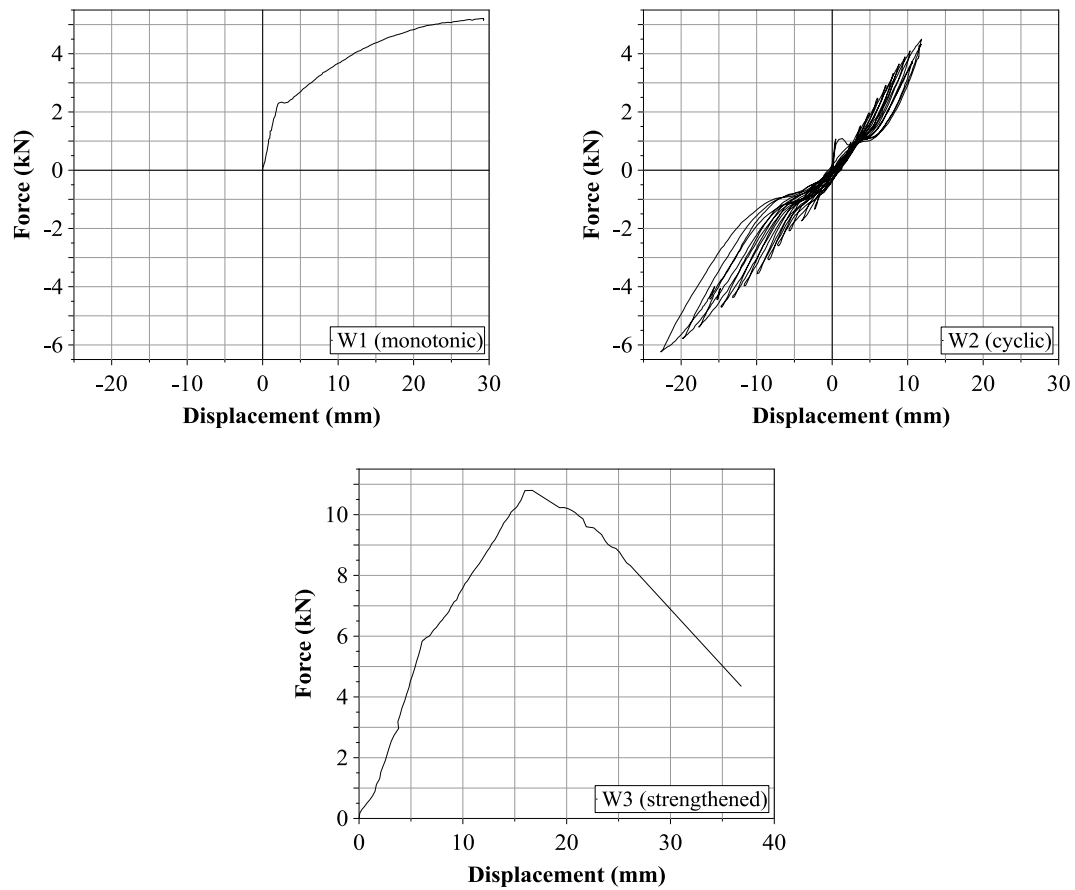


Figure 5. Force–displacement response comparison for phase I tests.

Table 2. Summary of force–displacement data for phase I tests.

Specimen	F_{cr} (kN)	Δ_{cr} (mm)	F_{max} (kN)	$\Delta_{F_{max}}$ (mm)	
W1	2.34	2.45	5.21	29.26	
W2	dir. (+)	1.10	1.18	4.50	11.85
	dir. (-)	-1.74	-4.06	-6.24	-22.71
W3	5.86	6.16	10.79	16.69	

Regarding the failure modes, one-way vertical out-of-plane bending was observed for control specimens W1 and W2. Material crushing was restricted to the weak mortar joints. In particular, flexural tensile cracks formed at the bed joints right below and right above the wall mid-height respectively (see Figures 6a and 6b) where the maximum strain is concentrated. Increasing displacements led to further crack propagation and widening, with the maximum crack width observed during the tests reaching approximately 12 mm.

The strengthened specimen W3 exhibited a slightly different crack pattern (see Figure 6c). As in the case of the monotonically tested W1, initially a main flexural tensile crack formed at the bed joint right below the wall mid-height. However, further crack propagation and widening was distinctly delayed due to the beneficial effect of the strengthening technique. In the course of the test, the aforementioned crack propagated across the wall thickness and reached a maximum width of about 7 mm. In addition, the pattern was supplemented by: (a) a stepped crack at the bottom course of the front side, (b) a horizontal crack along the bed joint above the bottom course of the back side, and (c) a group of diagonal cracks extending at the lower half of the two vertical edges, all indications of the increased axial stressing of the wall.

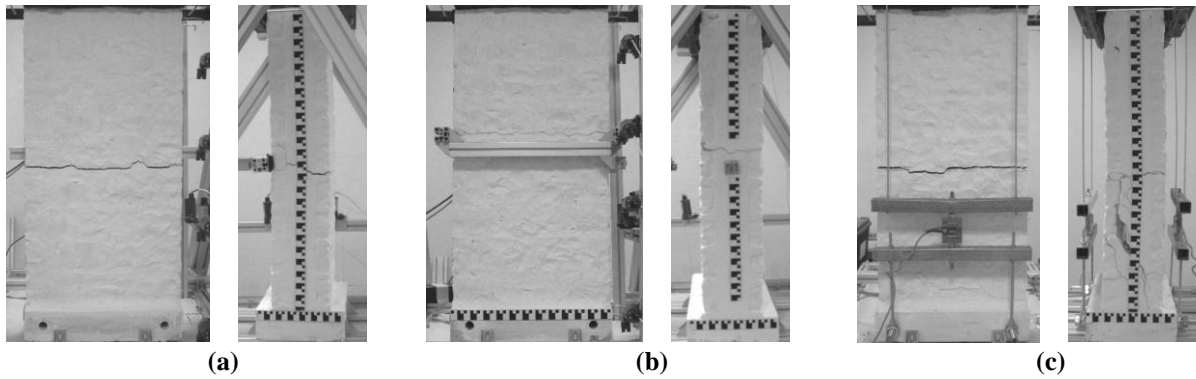


Figure 6. Post-test crack patterns observed on specimen: (a) W1, (b) W2, and (c) W3.

5.2. Phase II tests: considering SFSI effects

Figure 7 presents the force–displacement (at wall mid-height) response obtained during phase II tests, while the corresponding key data are summarized in Table 3. As expected, the initial linear-elastic response stage was followed by post-cracking cycles associated with strength and stiffness degradation, as a result of damage accumulation. Nevertheless, the results reveal that the performance of the walls was substantially affected by soil–foundation–structure interaction. The wall founded on dense sand exhibits higher strength than the one on loose sand. However, it is worthy to note that the residual strength of the wall seems to be independent of the soil stiffness. The walls exhibited substantial displacement capacity, as they were pushed to displacements close to the external leaf thickness (i.e., 67 mm); the maximum recorded displacements (Δ_{max}) were well in excess of the displacements at which cracking took place and peak force was attained (Δ_{cr}). It should be noted that the comparative test results of phases I and II, verify the sensitivity of the out-of-plane behavior of the walls to the boundary conditions. As expected, due to the beneficial effect of the additional axial load induced by the top support, specimens W1 and W2 significantly outperformed specimens W4 and W5. More specifically, while specimens W1 and W2 showed an increasing strength with displacement, specimens W4 and W5 exhibit degradation on both strength and stiffness.

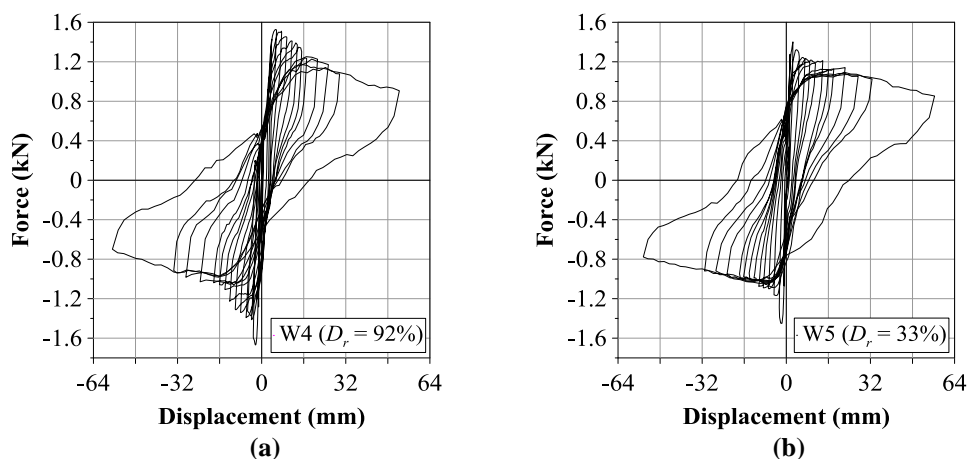


Figure 7. Force–displacement response for phase II tests: (a) dense sand, and (b) loose sand.

With respect to the failure modes, one-way vertical out-of-plane bending was observed for both walls. The post-test crack patterns can be seen in Figure 8. Material crushing was limited to the weak mortar joints, while the stones themselves remained elastic. Flexural tensile cracks formed at the bed joints right below and right above the wall mid-height. Further crack propagation and widening took place in the course of sequential loading cycles. The maximum crack width observed during the tests was about 35 mm for specimen W4, and 39 mm for specimen W5 respectively. It should be noted that the sustained damage was so extensive that the walls almost failed due to partial out-of-plane collapse.

Table 3. Summary of force–displacement data for phase II tests.

Specimen		F_{cr} (kN)	Δ_{cr} (mm)	$F_{\Delta max}$ (kN)	Δ_{max} (mm)
W4	dir. (+)	1.52	5.66	0.91	52.44
	dir. (-)	-1.67	-2.36	-0.71	-56.90
W5	dir. (+)	1.40	2.52	0.86	56.39
	dir. (-)	-1.46	-1.86	-0.78	-54.38



Figure 8. Post-test crack patterns observed on specimen: (a) W4, and (b) W5.

Figure 9 presents comparative test results associated with soil–foundation interaction, in terms of: (a) footing settlement–rotation response, (b) evolution of footing settlement in time, and (c) post-test soil deformation, as measured along the mid-axis of the footing. Note that settlement is denoted positive.

A combination of foundation rocking and soil bearing capacity mobilization was observed. The recorded time history of footing settlement verified that sequential loading cycles lead to settlement accumulation underneath the footings. As expected, soil resilience has a substantial influence on the performance of the soil–foundation–wall system.

Besides the obvious difference in the amount of settlement, the two soil materials reveal another disparity in their behavior: evidently, the footing on the dense sand layer experiences significant uplifting at each loading cycle, indicated by the ascending slope of the settlement–rotation ($w-\theta$) curves of Figure 9a [the gradient of $w-\theta$ curve indicates whether the foundation midpoint loses contact with the supporting soil as the foundation rotates, giving evidence on the amount of uplift that takes place during the test]. On the contrary, specimen W5 exhibits a *sinking* response. Interestingly however, the $w-\theta$ gradient of the latter foundation reverses after a few cycles of loading, showing upward movement of the foundation midpoint, and hence reduction of the minimum soil–foundation contact area, possibly as a result of sand densification (i.e., compaction) under the oscillating footing.

Foundation rocking gradually led to loss of contact between the soil and the footing close to its edges, where intense uplifting took place, in the case of dense sand. The formed gap, where the footing is detached from the underlying soil, is clearly visible in the close-up photo of Figure 10a which was taken after test completion. Inspection of Figure 9c reveals a recorded arc-shaped soil surface formation beneath the footing of specimen W4. The specific finding proves that the gaps generated at the front and the back of the footing were associated with a reduction of its effective width. The aforementioned phenomenon did not take place in the case of loose sand, where the performance was sinking-dominated. The close-up photo of Figure 10b illustrates that at the end of the test the footing was partially embedded in the loose soil.

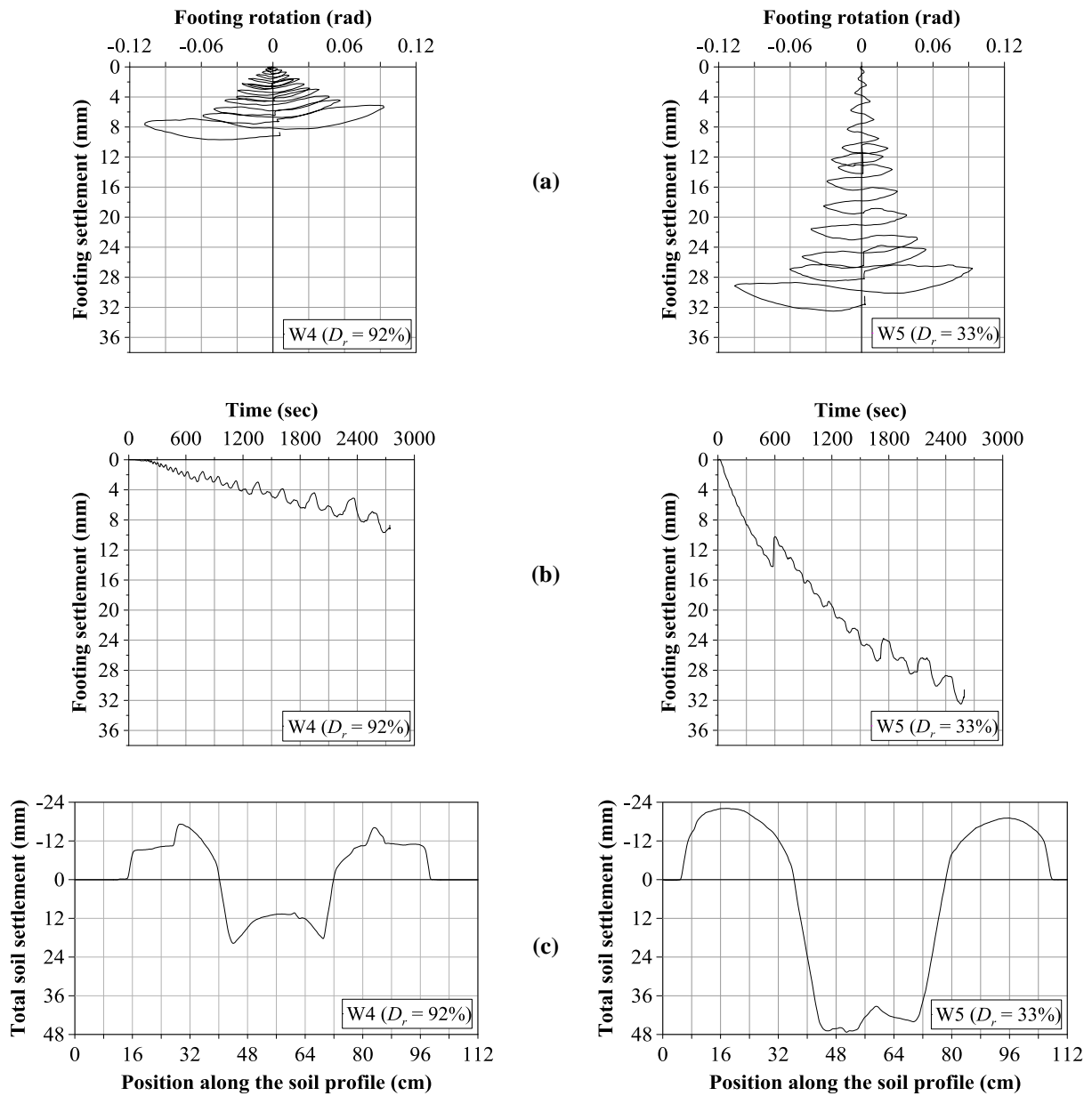


Figure 9. Comparative results for phase II tests: (a) footing settlement–rotation response, (b) time history of footing settlement, and (c) post-test soil deformation profile.

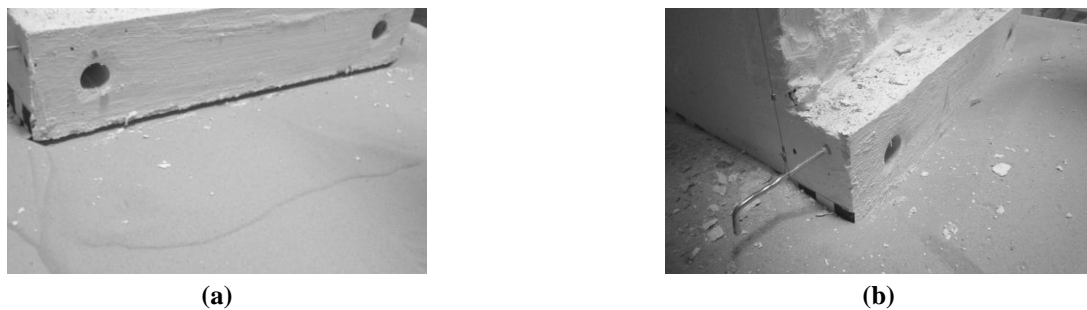


Figure 10. Post-test footing close-up photos: (a) dense sand (evident generated gap), and (b) loose sand.

6. CONCLUSIONS

An overview of the main results obtained through an experimental study on the out-of-plane response of historic three-leaf stone masonry walls has been presented in this paper. The effect of the following parameters was primarily investigated: (a) wall boundary conditions, and (b) soil–foundation–structure interaction (SFSI). The contribution of the study to knowledge enhancement in the field is underlined by the fact that no equivalent results have been reported in literature.

The out-of-plane response of the tested masonry walls exhibited high sensitivity to the boundary conditions. In the cases where the wall was not allowed to elongate, the additional axial load induced by the top support restraint resulted in significant enhancement of its out-of-plane capacity.

The obtained test results showed that the performance of such walls is substantially affected by soil–foundation–structure interaction (SFSI). Soil resilience had an essential effect on the system response. Combined bearing capacity mobilization and rocking of the foundation was observed. In the case of dense sand ($D_r = 92\%$), foundation rocking progressively led to a reduction of the soil–footing contact area (i.e., effective width), while, in the case of loose sand ($D_r = 33\%$) the response was governed by sinking.

Strengthening achieved by means of a post-tensioning system, proved to be highly effective against out-of-plane seismic actions. As expected, the strengthened wall significantly outperformed the control walls which were tested as built. In particular, its out-of-plane bearing capacity was practically doubled.

Furthermore, useful observations were made in regards with the manifested failure modes. The walls generally exhibited crack patterns associated with one-way vertical out-of-plane bending, with material crushing being restricted to the weak mortar joints.

ACKNOWLEDGEMENT

This work forms part of the EU research project “DARE” which is funded through the European Research Council’s (ERC) “IDEAS” Programme, in Support of Frontier Research–Advanced Grant, under contract/number ERC–2–9–AdG228254–DARE.

REFERENCES

- ABK (1981). Methodology for Mitigation of Seismic Hazards in Existing Unreinforced Masonry Buildings: Wall Testing, Out-of-Plane. ABK Topical Report 04. *Technical Report*. ABK, El Segundo, California.
- Anastasopoulos, I., Georgarakos, P., Georgiannou, V., Drosos, V., Kourkoulis, R. (2010). Seismic Performance of Bar-Mat Reinforced-Soil Retaining Wall: Shaking Table Testing versus Numerical Analysis with Modified Kinematic Hardening Constitutive Model. *Journal of Soil Dynamics and Earthquake Engineering*. **30**: 1089–1105.
- Derakhshan, H. and Ingham, J.M. (2008). Out-of-plane testing of an unreinforced masonry wall subjected to one-way bending. *Australian Earthquake Engineering Conference*. Ballarat, Victoria, Australia.
- Griffith, M.C., Lam, N.T.K., Wilson, J.L., Doherty, K. (2004). Experimental investigation of unreinforced brick masonry walls in flexure. *Journal of Structural Engineering*. **130**:3, 423–432.
- Griffith, M.C., Vaculik, J., Lam, N.T.K., Wilson, J., Lumantarna, E. (2007). Cyclic testing of unreinforced masonry walls in two-way bending. *Journal of Earthquake Engineering and Structural Dynamics*. **36**:6, 801–821.
- Kanit, R. and Atimtay, E. (2006). Experimental Assessment of the Seismic Behavior of Load-Bearing Masonry Walls Loaded Out-of-Plane. *Turkish Journal of Engineering and Environmental Sciences*. **30**:2, 101–113.
- Meisl, C. S., Elwood, K. J. and Ventura C. E. (2007). Shake table tests on the out-of-plane response of unreinforced masonry. *Canadian Journal of Civil Engineering* **34**:11, 1381–1392.
- Wilhelm, M., Mojsilovic, N. and Dazio, A. (2007). Out-of-Plane Shaking Table Tests on Unreinforced Masonry Walls. *10th North American Masonry Conference*. St. Louis, Missouri, USA.